2

Dynamical Systems Background

The need for a universal language:
from steady patterns to turbulence

Fluid transitions, such as those described in the previous chapter, are associated with the change in stability of flow patterns. Intuitively, an equilibrium flow (such as the Couette flow in the Taylor–Couette problem of Section 1.3) is stable when initial perturbations to the flow decay to zero in time. When critical values of parameters, such as the Reynolds numbers in the Taylor–Couette problem, are exceeded, perturbations on the flow will grow in time and eventually lead to a different equilibrium flow. In this chapter, we provide the background of this stability problem in the language of dynamical systems theory. It is written mostly as a refresher and to define the terminology which will be used in later chapters.

2.1 Stability of Fluid Flows

A general framework on the loss of stability of a fluid flow is given in Landau and Lifshitz (1987).

2.1.1 Stability Boundaries

We follow Joseph (1976) on stability boundaries, using the concept of asymptotic stability in the mean. Consider a constant-density (ρ) steady flow with an equilibrium velocity field $\bar{\mathbf{u}}$, referred to as the basic state, in a fixed flow domain $\mathcal{V}$. For a velocity perturbation $\tilde{\mathbf{u}}$ on $\bar{\mathbf{u}}$, the volume-averaged perturbation kinetic energy $\mathcal{E}$ is given by

$$\mathcal{E}(t) = \int_{\mathcal{V}} \frac{\rho}{2} \left\|\tilde{\mathbf{u}}\right\|^2 d^3x. \tag{2.1}$$

https://doi.org/10.1017/9781108863148.003 Published online by Cambridge University Press

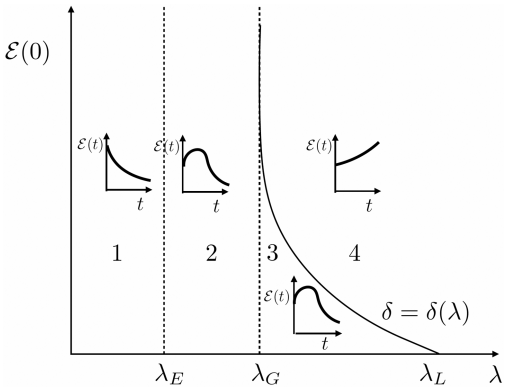

Figure 2.1 Plot of the different stability regimes, with 1: monotonic stability, 2: global stability, 3: conditional stability, and 4: instability. The control parameter is λ and the values of λ_E, λ_G, and λ_L are the energy, global, and linear stability boundaries, respectively. The curve $\delta(\lambda)$ bounds the region of conditional stability. Typical trajectories of the volume-averaged perturbation kinetic energy are sketched to illustrate the different behaviour in each domain.

For isothermal flows, such as the Lid-Driven Cavity flow and the Taylor–Couette flow, an equation for $\mathcal{E}$ can be obtained from the mechanical energy balance equation (Joseph, 1976).

The solution $\bar{\mathbf{u}}$ is said to be asymptotically stable in the mean if

$$\lim_{t\to\infty} \frac{\mathcal{E}(t)}{\mathcal{E}(0)} = 0, \tag{2.2}$$

where $\mathcal{E}(0)$ is the initial value of $\mathcal{E}$ at $t = 0$. If there exists a positive constant δ such that (2.2) holds only when $\mathcal{E}(0) < \delta$, then the basic state is said to be conditionally stable. If $\delta \to \infty$, then the basic state is globally stable; and if (2.2) is satisfied and $d\mathcal{E}(t)/dt < 0$ holds for all $t > 0$, then the basic state is said to be monotonically stable. Note that this definition of stability does not a priori assume that the perturbations should be small compared to the basic state.

Let one of the parameters in a particular model be indicated by λ, for example, the Reynolds number in the Lid-Driven Cavity flow. Based on the concept of asymptotic stability in the mean, four regions can be distinguished (Fig. 2.1):

- In region 1, the basic state is monotonically stable; all perturbations, whatever their initial amplitude, have a monotonically decaying perturbation kinetic energy.
- In region 2, there may be perturbations which initially grow (not necessarily exponentially), but the perturbation kinetic energy eventually decays to zero for all initial amplitudes of the perturbations.

https://doi.org/10.1017/9781108863148.003 Published online by Cambridge University Press

- Region 3 is a region of conditional instability. If the initial amplitude of the perturbations is small enough ($\mathcal{E}(0) < \delta(\lambda)$), the perturbation kinetic energy decays to zero, whereas if it is larger than some particular value $\delta(\lambda)$, the perturbation kinetic energy will increase. In the latter case, the perturbed state will evolve to a different state (than $\bar{\mathbf{u}}$), and the state $\bar{\mathbf{u}}$ is said to be (non-linearly) unstable to finite amplitude perturbations.
- In region 4, even infinitesimally small perturbations grow and the basic state is said to be (linearly) unstable.

From Fig. 2.1, stability boundaries have been defined (Joseph, 1976) according to the evolution of the perturbation kinetic energy $\mathcal{E}$. When $\lambda < \lambda_G$, then the basic state is globally stable and every perturbation decays to zero in time; λ_G is the global stability boundary and provides *sufficient conditions for stability*. If $\lambda < \lambda_E$, the basic state is monotonically stable; λ_E is called the energy stability boundary. If $\lambda_G < \lambda < \lambda_L$, then the basic state is conditionally stable: small amplitude disturbances decay, whereas excessively large perturbations grow. Beyond the linear stability boundary λ_L, infinitesimally small perturbations will grow, and this stability bound therefore provides *sufficient conditions for instability*. In summary, there are two cases of instability:

(i) Sub-critical instability: $\lambda_G < \lambda < \lambda_L$, the basic state is not globally stable.
(ii) Super-critical instability: $\lambda > \lambda_L$, the basic state is not linearly stable.

The linear stability boundary is obtained by linearizing the governing equations for the perturbations in their infinitesimally small amplitude. This linear stability problem leads to an eigenvalue problem which, except in some specific cases, also has to be solved numerically.

Additional Material

- Determination of the global and energy stability boundaries has to be done with the full non-linear equations. Use is made of variational principles, and many examples, also for the flows in Chapter 1, are provided in Joseph (1976) and Straughan (2004).

2.1.2 Linear Stability Boundary: An Example

As an example of a linear stability boundary, we present the famous (Rayleigh, 1916) result for pure Rayleigh–Bénard flow in a horizontally unbounded rectangular container ($A_x \to \infty, A_y \to \infty$) where the two horizontal solid walls are assumed to satisfy slip boundary conditions.

https://doi.org/10.1017/9781108863148.003 Published online by Cambridge University Press

The governing equations (Section 1.4), for $Ma = 0, Bi \to \infty$, are non-dimensionalized using scales κ/D for velocity, D^2/κ for time, and D for length. Moreover, a dimensionless temperature ϑ is introduced through $T = (T_B - T_A)\vartheta + T_A$ and a dimensionless pressure P through $p = -g\rho_0 z + (\mu\kappa/D^2)P$, where the first term is the hydrostatic component. This leads to the non-dimensional problem

$$Pr^{-1}\left(\frac{\partial \mathbf{u}}{\partial t} + \mathbf{u}\cdot\nabla\mathbf{u}\right) = -\nabla P + \nabla^2\mathbf{u} + Ra\,\vartheta\,\mathbf{e}_3, \tag{2.3a}$$

$$\nabla\cdot\mathbf{u} = 0, \tag{2.3b}$$

$$\frac{\partial \vartheta}{\partial t} + \mathbf{u}\cdot\nabla\vartheta = \nabla^2\vartheta, \tag{2.3c}$$

where $\mathbf{e}_3$ is the unit vector in vertical direction and with boundary conditions

$$z = 0\colon \vartheta = 1\ ;\ \frac{\partial u}{\partial z} = \frac{\partial v}{\partial z} = w = 0, \tag{2.4a}$$

$$z = 1\colon \frac{\partial u}{\partial z} = \frac{\partial v}{\partial z} = w = \vartheta = 0. \tag{2.4b}$$

In Equations (2.3)–(2.4), the two dimensionless parameters Pr (Prandtl) and Ra (Rayleigh) appear which are defined as

$$Ra = \frac{\alpha_T g(T_B - T_A)D^3}{\nu\kappa}\ ;\ Pr = \frac{\nu}{\kappa}.$$

The dimensionless motionless solution (the basic state) is given by

$$\bar{u} = \bar{v} = \bar{w} = 0\ ;\ \bar{\vartheta}(z) = 1 - z, \tag{2.5a}$$

$$\bar{P}(z) = Ra(z - \frac{z^2}{2}), \tag{2.5b}$$

being a solution for all values of Ra and Pr.

Infinitesimal perturbations on this basic state are assumed next, that is, $u = \bar{u} + \tilde{u}$ with similar expressions for the other variables, where the tilde indicates the perturbation quantities. Linearizing the equations around the background state (neglecting products of perturbation terms) leads to

$$Pr^{-1}\frac{\partial \tilde{\mathbf{u}}}{\partial t} = -\nabla\tilde{P} + \nabla^2\tilde{\mathbf{u}} + Ra\,\tilde{\vartheta}\,\mathbf{e}_3, \tag{2.6a}$$

$$\nabla\cdot\tilde{\mathbf{u}} = 0, \tag{2.6b}$$

$$\frac{\partial \tilde{\vartheta}}{\partial t} - \tilde{w} = \nabla^2\tilde{\vartheta} \tag{2.6c}$$

with boundary conditions

$$z = 0, 1\colon \frac{\partial \tilde{u}}{\partial z} = \frac{\partial \tilde{v}}{\partial z} = \tilde{w} = \tilde{\vartheta} = 0. \tag{2.7}$$

https://doi.org/10.1017/9781108863148.003 Published online by Cambridge University Press

Next, a normal mode expansion is employed, that is, for $\tilde{w}$, *See example Ex. 2.1*

$$\tilde{w} = e^{\sigma t} H(\mathbf{x}) W(z), \tag{2.8a}$$

$$H(\mathbf{x}) = \sum_{j=-N, j\neq 0}^{j=N} \mathbf{c}_j e^{i\mathbf{k}_j \cdot \mathbf{x}}, \tag{2.8b}$$

with similar expressions for the other quantities. Here $\mathbf{x} = (x, y, 0)$ and $\mathbf{k} = (k_x, k_y, 0)$ are the horizontal coordinate and wavenumber vector, respectively. The wavenumber vectors $\mathbf{k}_j$ differ only in orientation, $\mathbf{k}_{-j} = -\mathbf{k}_j$, $\mathbf{c}_{-j} = \mathbf{c}_j^*$ (where the $*$ indicates the complex conjugate) and $|\mathbf{k}_j| = k$. The function H represents possible two-dimensional space-filling patterns such as roll cells and hexagons.

Expressing $\tilde{P}, \tilde{u}, \tilde{v}$, and $\tilde{\vartheta}$ in terms of $\tilde{w}$ using the equations in (2.6) leads to the following problem (Getling, 1998):

$$\frac{\partial^2 H}{\partial x^2} + \frac{\partial^2 H}{\partial y^2} + k^2 H = 0, \tag{2.9a}$$

$$(D_z^2 - k^2 - \sigma)(D_z^2 - k^2 - \frac{\sigma}{Pr})(D_z^2 - k^2) W = -k^2 Ra\, W, \tag{2.9b}$$

where $D_z = d/dz$. The boundary conditions for W become

$$W(0) = W(1) = D_z^2 W(0) = D_z^2 W(1) = D_z^4 W(0) = D_z^4 W(1) = 0. \tag{2.10}$$

The eigenfunctions for W are given by

$$W_n(z) = \sin n\pi z, n = 1, 2, \ldots \tag{2.11}$$

and the eigenvalues σ (labelled by the vertical structure of the eigenfunctions) are given by

$$\sigma_n = -\frac{Pr+1}{2}(n^2\pi^2 + k^2) \pm \sqrt{(\frac{Pr-1}{2})^2 (n^2\pi^2 + k^2)^2 + \frac{RaPrk^2}{n^2\pi^2 + k^2}}. \tag{2.12}$$

As $Ra \geq 0$, the eigenvalues are real and there is always a positive eigenvalue when

$$Ra > Ra_n(k) = \frac{(n^2\pi^2 + k^2)^3}{k^2}. \tag{2.13}$$

The so-called neutral curve for $n = 1$ ($\sigma_1 = 0$), showing $Ra_1(k)$ versus k, is plotted in Fig. 2.2. This curve has a minimum at (k_c, Ra_c) given by

$$k_c = \frac{\pi}{\sqrt{2}}\ ;\ Ra_c = \frac{27}{4}\pi^4. \tag{2.14}$$

Hence, for $Ra > Ra_c$, there is a band of wavenumbers with $\sigma > 0$ and so these perturbations will grow exponentially. The value of Ra_c therefore provides sufficient conditions for instability and is the linear stability boundary. Note that multiple patterns (hexagons, rolls, represented by the function $H(x, y)$) become unstable under

https://doi.org/10.1017/9781108863148.003 Published online by Cambridge University Press

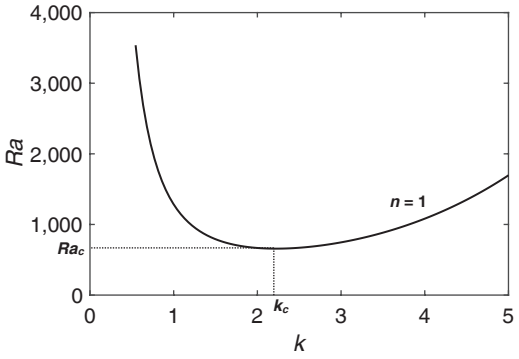

Figure 2.2 Neutral curve for pure Rayleigh–Bénard convection, showing $Ra_1(k)$ from (2.13) versus k (for $\sigma_1 = 0$) in a horizontally unbounded rectangular liquid layer with slip conditions at the top and bottom walls.

the same conditions, as the stability boundary depends only on the norm k of the wavenumber vector $\mathbf{k}$. *See example Ex. 2.2*

Additional Material

- Linear stability theory of fluid flows is standard material in textbooks on hydrodynamic stability theory, such as Chandrasekhar (1961) and Drazin and Reid (2004).
- Specific focus on the stability of the Rayleigh–Bénard–Marangoni flow and related flows can be found in Getling (1998) and Platten and Legros (1984).

2.2 Beyond Criticality: Weakly Non-linear Theory

When the control parameter λ is slightly above the linear stability boundary λ_c, such as $Ra > Ra_c$ in the Rayleigh–Bénard problem of the previous subsection, a band of wavenumbers destabilizes the basic flow as the associated spatial patterns grow exponentially in time. At some later time, the linear theory is no longer valid because the amplitude of the non-linear terms can no longer be neglected. In this section, the so-called weakly non-linear theory is presented where non-linear effects are taken into account in the regime

$$\frac{|\lambda - \lambda_c|}{|\lambda_c|} < \epsilon, \tag{2.15}$$

where $\epsilon \ll 1$.

When at least one of the horizontal dimensions is unbounded, and hence the importance of boundary conditions in this direction on the finite amplitude flows

https://doi.org/10.1017/9781108863148.003 Published online by Cambridge University Press

is neglected, the weakly non-linear analysis leads to a Ginzburg–Landau equation. When the effects of horizontal boundary conditions cannot be neglected, the weakly non-linear approach will lead to a set of amplitude equations. We will describe both approaches in what follows for a general flow problem for the state vector $\mathbf{\Phi}$ (e.g., $\mathbf{u}, p$) with governing equations

$$\mathcal{M}\frac{\partial \mathbf{\Phi}}{\partial t} + \mathcal{G}(\mathbf{\Phi}) = \mathbf{f}, \tag{2.16}$$

with appropriate boundary conditions on the boundary of the flow domain. Here $\mathcal{M}$ is a linear operator, $\mathcal{G}$ is a non-linear operator, and $\mathbf{f}$ represents the forcing. Note that the operator $\mathcal{M}$ does not need to the identify, as in the incompressible general fluid dynamics equations there is an equation without a time derivative (i.e., the continuity equation).

2.2.1 Ginzburg–Landau Equations

Consider first the case where one of the horizontal dimensions of the problem is unbounded, which allows the existence of traveling wave solutions of the linear stability problem. The background state $\bar{\mathbf{\Phi}}$ is assumed to be steady and satisfies

$$\mathcal{G}(\bar{\mathbf{\Phi}}) = \mathbf{f}. \tag{2.17}$$

We next now consider perturbations $\boldsymbol{\phi} = \mathbf{\Phi} - \bar{\mathbf{\Phi}}$, and the system of equations for the perturbations $\boldsymbol{\phi}$ can be written in general as

$$(\mathcal{M}\frac{\partial}{\partial t} + \mathcal{L})\boldsymbol{\phi} + \mathcal{N}(\boldsymbol{\phi})\boldsymbol{\phi} = 0 \tag{2.18}$$

with appropriate boundary conditions. Here $\mathcal{L}$ is a linear operator and $\mathcal{N}$ a non-linear operator which we assume to represent a quadratic non-linearity (as in the governing equations in Section 1.1). The linear stability problem (where non-linear interactions of the perturbations are neglected) is formulated as

$$(\mathcal{M}\frac{\partial}{\partial t} + \mathcal{L})\tilde{\boldsymbol{\phi}} = 0 \tag{2.19}$$

for infinitesimally small perturbations $\tilde{\boldsymbol{\phi}}$.

Assume that the x-direction is unbounded such that traveling wave solutions of (2.19) exist with wavenumber k and complex growth factor σ. For convenience, we will consider the two-dimensional Cartesian case (coordinates (x, z)), with

$$\tilde{\boldsymbol{\phi}}(x, z, t) = \hat{\boldsymbol{\phi}}(z)e^{ikx+\sigma t} + c.c. \tag{2.20}$$

where $c.c.$ indicates complex conjugate. Substitution of (2.20) into (2.19) gives a boundary value problem for the eigenpair $(\sigma, \hat{\boldsymbol{\phi}})$, that is,

$$(\hat{\mathcal{M}}(k)\sigma + \hat{\mathcal{L}}(k))\hat{\boldsymbol{\phi}} = 0 \tag{2.21}$$

https://doi.org/10.1017/9781108863148.003 Published online by Cambridge University Press

with appropriate boundary conditions. Here the operators $\hat{\mathcal{M}}$ and $\hat{\mathcal{L}}$ are the Fourier transforms of the original operators in the x-direction.

The eigenvalue is written as $\sigma = \sigma_R + i\sigma_I$ and considered as a function of the wavenumber k and the control parameter λ. The neutral curve $\sigma_R(k,\lambda) = 0$ provides sufficient conditions for instability, and in many applications, the neutral curve has a minimum at (k_c, λ_c) (see Fig. 2.2) at which

$$\sigma_R(k_c,\lambda_c) = 0\ ;\ \frac{\partial\sigma_R}{\partial k}(k_c,\lambda_c) = 0\ ;\ \frac{\partial^2\sigma_R}{\partial k^2}(k_c,\lambda_c) < 0. \tag{2.22}$$

In what follows we will use $\omega_c = \sigma_I(k_c)$, and also assume that the mode $k = 0$ is damped.

Assume now conditions just above criticality, that is,

$$\lambda = \lambda_c + m\epsilon^2, \tag{2.23}$$

where $\epsilon \ll 1$ and $m = \mathcal{O}(1)$. As the neutral curve can be approximated by a parabola $\lambda - \lambda_c \sim (k-k_c)^2$, this implies that $|k-k_c| = \mathcal{O}(\epsilon)$. The unstable traveling waves are hence limited to a narrow band around k_c which can be interpreted as a wave packet with central wavenumber k_c. This wave packet evolves on a time scale which is large compared to typical wave periods $2\pi/\omega_c$ and is characterized by scales

$$T = \epsilon^2 t\ ;\ X = \epsilon(x - c_g t), \tag{2.24}$$

where $c_g = \partial\sigma_I/\partial k$ is the group velocity. The long spatial variable X is a slowly moving coordinate, traveling with the group velocity of the growing wave packet.

The scaling leads to transformations for $\boldsymbol{\phi}(x, X(x,t), z, t, T(t))$ as

$$\frac{\partial}{\partial t} \rightarrow \frac{\partial}{\partial t} - \epsilon c_g \frac{\partial}{\partial X} + \epsilon^2 \frac{\partial}{\partial T}, \tag{2.25a}$$

$$\frac{\partial}{\partial x} \rightarrow \frac{\partial}{\partial x} + \epsilon \frac{\partial}{\partial X}. \tag{2.25b}$$

The final amplitude of the perturbations will be small compared to that of the background state (for λ close to λ_c), so the solution vector is expanded in terms of the small parameter ϵ and Fourier modes of the marginally stable wave $E = \exp(i(k_c x + \omega_c t))$, that is,

$$\boldsymbol{\phi} = \epsilon\boldsymbol{\Phi}^{(11)}E + \epsilon^2(\boldsymbol{\Phi}^{(02)} + \boldsymbol{\Phi}^{(12)}E + \boldsymbol{\Phi}^{(22)}E^2) + \epsilon^3\boldsymbol{\Phi}^{(13)}E + \ldots + c.c. \tag{2.26}$$

where the $\boldsymbol{\Phi}^{(ij)} = \boldsymbol{\Phi}^{(ij)}(X, z, T)$ depend on the slow time scale and long spatial scale.

Substitution of (2.26) into (2.18) and collecting terms of the same order (in ϵ and E) gives at $\mathcal{O}(\epsilon E)$ the linear stability problem

https://doi.org/10.1017/9781108863148.003 Published online by Cambridge University Press

$$(i\omega_c\hat{\mathcal{M}}(k_c)+\hat{\mathcal{L}}(k_c))\mathbf{\Phi}^{(11)}=0. \tag{2.27}$$

As the left-hand side does not operate on the large scales of X and T, we can write $\mathbf{\Phi}^{(11)}=A(X,T)\mathbf{\Psi}$, where $\mathbf{\Psi}=\hat{\boldsymbol{\phi}}(z)$ is the eigenvector at $k=k_c$ from (2.20) and (2.20). The weakly non-linear analysis eventually leads to an equation for the scalar (but complex) amplitude $A(X,T)$. At $\mathcal{O}(\epsilon^2 E)$, the equations are

$$(i\omega_c\hat{\mathcal{M}}(k_c)+\hat{\mathcal{L}}(k_c))\mathbf{\Phi}^{(12)}=-(i\omega_c\hat{\mathcal{M}}_k(k_c)+\hat{\mathcal{L}}_k(k_c)-c_g\hat{\mathcal{M}}(k_c))\frac{\partial\mathbf{\Phi}^{(11)}}{\partial X}, \tag{2.28}$$

where the subscript k indicates differentiation to k. At $\mathcal{O}(\epsilon^2)$ and $\mathcal{O}(\epsilon^2E^2)$, one finds

$$\hat{\mathcal{L}}(0)\mathbf{\Phi}^{(02)} = -2\mathcal{R}(\mathcal{N}(\mathbf{\Phi}^{(11)})\mathbf{\Phi}^{(11)*}), \tag{2.29a}$$

$$(2i\omega_c\hat{\mathcal{M}}(2ik_c)+\hat{\mathcal{L}}(2ik_c))\mathbf{\Phi}^{(22)} = -\mathcal{N}(\mathbf{\Phi}^{(11)})\mathbf{\Phi}^{(11)}, \tag{2.29b}$$

where $\mathcal{R}$ indicates real part and $*$ again complex conjugate. Using the relation $\mathbf{\Phi}^{(11)}=A(X,T)\mathbf{\Psi}$ in the equations of (2.28) and (2.29) leads to

$$\mathbf{\Phi}^{(12)}=\frac{\partial A}{\partial X}\mathbf{\Psi}^{(12)}\ ;\ \mathbf{\Phi}^{(02)}=|A|^2\mathbf{\Psi}^{(02)}\ ;\ \mathbf{\Phi}^{(22)}=A^2\mathbf{\Psi}^{(22)}, \tag{2.30}$$

where the vectors $\mathbf{\Psi}^{(12)}$, $\mathbf{\Psi}^{(02)}$, and $\mathbf{\Psi}^{(22)}$ satisfy

$$\begin{aligned}(i\omega_c\hat{\mathcal{M}}(k_c)+\hat{\mathcal{L}}(k_c))\mathbf{\Psi}^{(12)} &= -(i\omega_c\hat{\mathcal{M}}_k(k_c)+\hat{\mathcal{L}}_k(k_c)\\ &\quad -c_g\hat{\mathcal{M}}(k_c))\mathbf{\Psi}, \qquad (2.31a)\\ \hat{\mathcal{L}}(0)\mathbf{\Psi}^{(02)} &= -2\mathcal{R}(\mathcal{N}(\mathbf{\Psi})\mathbf{\Psi}^*), \qquad (2.31b)\\ (2i\omega_c\hat{\mathcal{M}}(2ik_c)+\hat{\mathcal{L}}(2ik_c))\mathbf{\Psi}^{(22)} &= -\mathcal{N}(\mathbf{\Psi})\mathbf{\Psi} \qquad (2.31c)\end{aligned}$$

and these equations are complemented with the appropriate boundary conditions at each order of the expansion.

Differentiation of the eigenvalue problem (2.21) to k and use of the group velocity at criticality gives $\mathbf{\Psi}^{(12)}$ from (2.31a) as

$$\mathbf{\Psi}^{(12)}=-i\frac{\partial\mathbf{\Psi}}{\partial k} \tag{2.32}$$

evaluated at criticality. The left-hand sides of (2.31b,c) are non-singular and hence can be solved for $\mathbf{\Psi}^{(02)}$ and $\mathbf{\Psi}^{(22)}$. At $\mathcal{O}(\epsilon^3E^2)$ a singular problem is obtained for $\mathbf{\Psi}^{(13)}$, that is,

$$(i\omega_c\hat{\mathcal{M}}(k_c)+\hat{\mathcal{L}}(k_c))\mathbf{\Psi}^{(13)}=-(\mathcal{M}(k_c)\mathbf{\Psi}\frac{\partial A}{\partial T}+m\mathbf{\Gamma}A+\mathbf{\Sigma}\frac{\partial^2A}{\partial X^2}+\mathbf{\Lambda}A|A|^2), \tag{2.33}$$

https://doi.org/10.1017/9781108863148.003 Published online by Cambridge University Press

where

$$\mathbf{\Gamma} = (\hat{\mathcal{L}}_\lambda(k_c) - i\omega_c\hat{\mathcal{M}}_\lambda(k_c))\mathbf{\Psi}, \tag{2.34a}$$

$$\mathbf{\Sigma} = \frac{1}{2}(i\omega_c\hat{\mathcal{M}}_{kk}(k_c) - \hat{\mathcal{L}}_{kk}(k_c) - 2c_g\hat{\mathcal{M}}_k(k_c))\mathbf{\Psi} + i(i\omega_c\hat{\mathcal{M}}_k(k_c) - c_g\hat{\mathcal{M}}(k_c) - \hat{\mathcal{L}}_k(k_c))\mathbf{\Psi}_k, \tag{2.34b}$$

$$\mathbf{\Lambda} = \mathcal{N}(\mathbf{\Psi})\mathbf{\Psi}^{(02)} + \mathcal{N}(\mathbf{\Psi}^{(02)})\mathbf{\Psi} + \mathcal{N}(\mathbf{\Psi}^{(22)})\mathbf{\Psi}^* + \mathcal{N}(\mathbf{\Psi}^*)\mathbf{\Psi}^{(22)}. \tag{2.34c}$$

See example Ex. 2.3

In general, the right-hand side of (2.33) is not contained in the range of the linear operator on the left-hand side. Since the kernel of the operator $i\omega_c\hat{\mathcal{M}}(k_c) + \hat{\mathcal{L}}(k_c)$ has dimension 1, it is spanned by one vector, here indicated by $\mathbf{\Omega}$; this implies that

$$\mathbf{\Omega}^H(i\omega_c\hat{\mathcal{M}}(k_c) + \hat{\mathcal{L}}(k_c))\mathbf{W} = 0, \tag{2.35}$$

where $\mathbf{W}$ is the right-hand side of (2.33) and the superscript H indicates Hermitian transposed. The resulting amplitude equation derived from (2.33) and (2.35) is the Ginzburg–Landau equation

$$\frac{\partial A}{\partial T} = \gamma_1 A + \gamma_2\frac{\partial^2 A}{\partial X^2} - \gamma_3 A|A|^2, \tag{2.36}$$

where

$$\gamma_1 = m\frac{\mathbf{\Omega}^H\mathbf{\Gamma}}{\mathbf{\Omega}^H\hat{\mathcal{M}}(k_c)\mathbf{\Psi}}, \tag{2.37a}$$

$$\gamma_2 = \frac{\mathbf{\Omega}^H\mathbf{\Sigma}}{\mathbf{\Omega}^H\hat{\mathcal{M}}(k_c)\mathbf{\Psi}}, \tag{2.37b}$$

$$\gamma_3 = -\frac{\mathbf{\Omega}^H\mathbf{\Lambda}}{\mathbf{\Omega}^H\hat{\mathcal{M}}(k_c)\mathbf{\Psi}}. \tag{2.37c}$$

In the remainder of the book, we will use the Ginzburg–Landau equation (2.36) as a one-dimensional partial differential equation for the complex amplitude $A(X, T)$ to illustrate bifurcation behaviour of typical fluid flows. As we will see, the behaviour of the solutions of this equation is very rich.

2.2.2 Amplitude Equations

In case the geometry of the problem is such that no traveling wave solutions exist (e.g., a bounded geometry in all directions), we can still obtain a reduced model near criticality through a Galerkin-type projection using the eigenfunctions of the linear operator.

Suppose that the original problem (2.16) is discretized (see Chapter 4) using a spectral, finite difference or finite element method. The set of discretized non-linear differential equations is rewritten in the general form,

https://doi.org/10.1017/9781108863148.003 Published online by Cambridge University Press

$$M\frac{d\mathbf{\Phi}}{dt} + L\mathbf{\Phi} + N(\mathbf{\Phi}, \mathbf{\Phi}) = \mathbf{f}, \tag{2.38}$$

to explicitly show the linear part L, the non-linear part N and the forcing $\mathbf{f}$. Let $\bar{\mathbf{\Phi}}$ be the solution to the steady problem, that is,

$$L\bar{\mathbf{\Phi}} + N(\bar{\mathbf{\Phi}}, \bar{\mathbf{\Phi}}) = \mathbf{f}. \tag{2.39}$$

The solution to (2.38) is now decomposed into this steady state and a remainder time-dependent part,

$$\mathbf{\Phi} = \bar{\mathbf{\Phi}} + \boldsymbol{\phi}. \tag{2.40}$$

After substitution into (2.38), the linearized flow $\boldsymbol{\phi}$ is governed by

$$M\frac{d\boldsymbol{\phi}}{dt} + J\boldsymbol{\phi} = 0, \tag{2.41}$$

where the total Jacobian J is defined as

$$J = L + N(\bar{\mathbf{\Phi}}, \cdot) + N(\cdot, \bar{\mathbf{\Phi}}). \tag{2.42}$$

The linear operators have an eigenvector decomposition,

$$\Lambda^H JR = \Sigma \; ; \; \Lambda^H MR = I. \tag{2.43}$$

Here R and Λ denote the right- and left-hand eigenspaces of the linear operator J, I is the identity, and the diagonal matrix Σ contains the corresponding eigenvalues, that is,

$$R = \begin{pmatrix} \mathbf{r}_1 & \mathbf{r}_2 & \cdots & \mathbf{r}_r \end{pmatrix}, \tag{2.44a}$$

$$\Lambda = \begin{pmatrix} \mathbf{l}_1 & \mathbf{l}_2 & \cdots & \mathbf{l}_r \end{pmatrix}, \tag{2.44b}$$

$$\Sigma = \mathrm{diag}(\sigma_1 \quad \sigma_2 \quad \cdots \quad \sigma_r), \tag{2.44c}$$

where $r = \mathrm{rank}(\Sigma) \leq d$, with d being the number of degrees of freedom of the dynamical system; the preceding inequality is due to the singular nature of M. Relation (2.43) states that Λ and R are a bi-orthogonal set of eigenvectors, and this property will be used in the Galerkin projection that follows.

With the use of this eigenbasis, the perturbation $\boldsymbol{\phi}$ is expanded in n right-hand eigenvectors:

$$\boldsymbol{\phi} = R_n a = \sum_{j=1}^{n} \mathbf{r}_j a_j(t). \tag{2.45}$$

The matrix R_n denotes the n-dimensional subspace of R of suitably chosen right-hand vectors, and Λ_n is its adjoint subspace.

https://doi.org/10.1017/9781108863148.003 Published online by Cambridge University Press

Substitution of (2.40) into (2.38) and using (2.39) and (2.45) yields

$$MR_n \frac{da}{dt} + JR_n a + N(R_n a, R_n a) = 0. \tag{2.46}$$

Projection onto the left-hand eigenbasis $\mathbf{\Lambda}_n$ and the use of the bi-orthogonality relation (2.43) results in the set of coupled amplitude equations,

$$\frac{da}{dt} - Sa + n(a, a) = \mathbf{0}. \tag{2.47}$$

The operators in the projected system are defined as

$$S = \Lambda_n^H J R_n, \tag{2.48a}$$
$$n(a, a) = \Lambda_n^H N(R_n a, R_n a). \tag{2.48b}$$

In terms of the individual components, the evolution of amplitudes $a_j(t), j = 1, \ldots, n$ is governed by

$$\frac{da_j}{dt} - \sum_{k=1}^{n} b_{jk} a_{jk} + \sum_{k=1}^{n} \sum_{l=1}^{n} c_{jkl} a_k a_l = 0 \quad , \quad j = 1, \ldots, n. \tag{2.49}$$

The coefficients in the projected system are defined as

$$b_{jk} = \mathbf{l}_j^H J \mathbf{r}_k, \tag{2.50a}$$
$$c_{jkl} = \mathbf{l}_j^H N(\mathbf{r}_k, \mathbf{r}_l). \tag{2.50b}$$

The main frustration with these amplitude equation models is the non-correspondence in dynamical behaviour between the reduced model and the full model when the order of truncation of the reduced model is changed (Van der Vaart *et al.*, 2002). An enormously rich behaviour may be found in many reduced models, which has fascinated researchers so much that critically examining the relation between the full and reduced models is often omitted. An example hereof is the famous Lorenz model (Lorenz, 1963), where the dynamics bear little resemblance to that of the underlying full model of Rayleigh–Bénard convection (Curry *et al.*, 1984). Hence, while this approach is fairly standard, the domain in parameter space where a close correspondence exists between the dynamical behaviour contained in (2.49), for a chosen value of n, and the full model is a priori unclear.

Additional Material

- Amplitude equations and the Ginzburg–Landau equation play an important role in theories in the broad research area of pattern formation; see Rabinovich *et al.* (2000) and Hoyle (2006).

https://doi.org/10.1017/9781108863148.003 Published online by Cambridge University Press

2.3 Dynamical Systems

The stability bounds do indicate where (in parameter space) flows become sensitive to perturbations, but do not give any answer on what new patterns can arise. Dynamical systems theory, and in particular bifurcation theory, is a systematic approach to determine which equilibrium flow patterns are possible near a stability boundary. Although dynamical systems theory can in general be formulated for infinite-dimensional systems, such as the Navier–Stokes equations, we present here the necessary concepts for finite-dimensional systems. The reason is that in a numerical approach, eventually (often high-dimensional) finite-dimensional dynamical systems are handled.

2.3.1 Continuous versus Discrete Systems

A general first-order system of ordinary differential equations (ODEs) can be written as the continuous time dynamical system

$$\frac{d\mathbf{x}}{dt} = \mathbf{f}(\mathbf{x}, \lambda, t), \tag{2.51}$$

where $\mathbf{x}$ is the state vector in the state space $\mathbb{R}^d$, $\mathbf{f}$ is a smooth (sufficiently differentiable) vector field, λ is a real parameter, and t denotes time. The number d is referred to as the dimension or the number of degrees of freedom of the dynamical system. When the vector field $\mathbf{f}$ does not depend explicitly on time, that is,

$$\frac{d\mathbf{x}}{dt} = \mathbf{f}(\mathbf{x}, \lambda), \tag{2.52}$$

the dynamical system is called autonomous; otherwise, it is called non-autonomous. A trajectory of the dynamical system, starting, for example, at $\mathbf{x}_0$, is a curve $\mathbf{x}(t)$ satisfying (2.51). Hence, at each point the vector field $\mathbf{f}$ is tangent to the curve and $\mathbf{x}(t)$ is a solution of the equations of (2.51).

When time is discrete, with counter k, we obtain a discrete dynamical system of the form

$$\mathbf{x}_{k+1} = \mathbf{f}_k(\mathbf{x}_k, \lambda). \tag{2.53}$$

A continuous time dynamical system can be analyzed as a discrete time dynamical system through a so-called Poincaré map. To define a Poincaré map, a hypersurface Σ^+ in the state space $\mathbb{R}^d$, for example a line segment in two-dimensional state space or a plane in three-dimensional state space, is chosen such that each trajectory is not tangent to it for all time t, that is, when

$$\mathbf{n} \cdot \mathbf{f} \neq 0. \tag{2.54}$$

https://doi.org/10.1017/9781108863148.003 Published online by Cambridge University Press

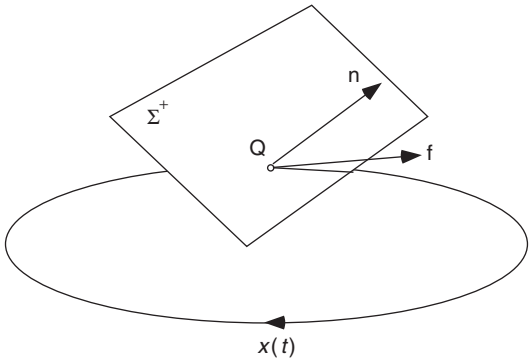

Figure 2.3 Sketch of a Poincaré section Σ^+. A periodic orbit is sketched which intersects the Poincaré section at the point Q. The vector **f** is the tangent to the trajectory at Q and **n** is the outward normal to Σ^+.

Here, **n** is the normal to the hypersurface (Fig. 2.3) and **f** the right-hand side of (2.51); this hypersurface is called a Poincaré section. Let a trajectory intersect a Poincaré section at successive intersections indicated by $\{\mathbf{x}_1, \mathbf{x}_2, \mathbf{x}_3, \ldots\}$; then the Poincaré map $\mathcal{P}\colon \Sigma^+ \to \Sigma^+$ is defined as

$$\mathbf{x}_{k+1} = \mathcal{P}\mathbf{x}_k. \tag{2.55}$$

2.3.2 Stability Theory of Fixed Points

A solution $\bar{\mathbf{x}} \in \mathbb{R}^d$ of an autonomous continuous dynamical system at a parameter value λ is a fixed point if

$$\mathbf{f}(\bar{\mathbf{x}}, \lambda) = 0, \tag{2.56}$$

and hence any trajectory with initial conditions on the fixed point will remain there forever. In this section, we are interested in the transient behaviour of small perturbations on such a fixed point.

In the analysis of the linear stability of a particular fixed point $\bar{\mathbf{x}}$, small perturbations **y** are assumed to be present, that is,

$$\mathbf{x} = \bar{\mathbf{x}} + \mathbf{y}, \tag{2.57}$$

and linearization of (2.52) around $\bar{\mathbf{x}}$ gives

$$\frac{d\mathbf{y}}{dt} = J(\bar{\mathbf{x}}, \lambda)\mathbf{y}, \tag{2.58}$$

where J is the Jacobian matrix given by

$$J = \begin{pmatrix} \frac{\partial f_1}{\partial x_1} & \cdots & \frac{\partial f_1}{\partial x_d} \\ \cdots & \cdots & \cdots \\ \frac{\partial f_d}{\partial x_1} & \cdots & \frac{\partial f_d}{\partial x_d} \end{pmatrix}. \tag{2.59}$$

https://doi.org/10.1017/9781108863148.003 Published online by Cambridge University Press

The solution of (2.58) with initial condition $\mathbf{y}_0$ is given by

$$\mathbf{y}(t) = e^{Jt}\mathbf{y}_0, \tag{2.60}$$

and hence the time behaviour depends on the eigenvalues of the Jacobian matrix J. The corresponding eigenvectors are usually referred to as the normal modes.

If J is decomposed as $J = U\Sigma U^{-1}$, where Σ contains the eigenvalues of J, e^{Jt} is given by

$$e^{Jt} = \sum_{k=0}^{\infty} \frac{1}{k!}(Jt)^k = U\left[\sum_{k=0}^{\infty} \frac{1}{k!}(\Sigma t)^k\right] U^{-1} = Ue^{\Sigma t}U^{-1}. \tag{2.61}$$

If all eigenvalues of J, say $\sigma_1, \ldots, \sigma_d$ have negative real parts, that is, $\mathcal{R}(\sigma_j) < 0$ for all j, then the fixed point is linearly stable. For this case, indeed all trajectories of (2.58) will approach $\mathbf{y} = 0$ asymptotically, that is, for $t \to \infty$. When at least one of the eigenvalues σ_k has a positive real part, $\mathcal{R}(\sigma_k) > 0$, the fixed point is said to be unstable.

2.4 Bifurcation Theory of Fixed Points

Bifurcation theory addresses changes in the qualitative behaviour of a dynamical system as one or several of its parameters vary. If J in (2.59) has no purely imaginary eigenvalues, $\bar{\mathbf{x}}$ is called a hyperbolic fixed point. Near such a fixed point, the local solution structure of the linearized system is the same as that of the non-linear system. This is a consequence of the so-called Hartman–Grobman theorem (Guckenheimer and Holmes, 1990). When qualitative changes occur in the fixed-point solutions of the dynamical system, such as the changes in type or number of solutions, the dynamical system is said to have undergone a bifurcation. This can only occur at non-hyperbolic fixed points. In the state-parameter space formed by $(\mathbf{x}, \lambda)$, locations at which bifurcations occur are called bifurcation points. A bifurcation that needs at least k parameters to occur is called a co-dimension-k bifurcation.

The center manifold theorem (Guckenheimer and Holmes, 1990) implies that it is possible to (locally) reduce the dynamics. Typically, taking $\bar{\mathbf{x}} = 0$ for simplicity, one has

$$\frac{d\mathbf{x}}{dt} = L\mathbf{x} + N(\mathbf{x}), \tag{2.62}$$

where N, which depends on the parameter λ, has a Taylor expansion starting with at least quadratic terms, $\mathbf{x} \in \mathbb{R}^m$ and L has m eigenvalues with zero real part. Having reduced the system (2.51) into the system (2.62), it is possible to find a change of coordinates so that the system becomes 'as simple as possible'. The resulting vector field thus obtained is called the normal form. This procedure is an extension of the reduction to Jordan form for matrices to the non-linear case. Normal form

https://doi.org/10.1017/9781108863148.003 Published online by Cambridge University Press

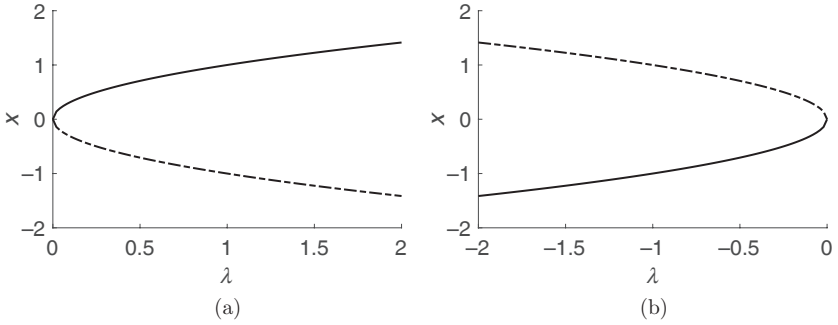

Figure 2.4 Super-critical (a) and sub-critical (b) saddle-node bifurcation. The solid (dash-dotted) branches indicate stable (unstable) solutions.

theory (Guckenheimer and Holmes, 1990) provides a way to classify the different kind of bifurcations that may occur with only knowledge of the eigenvalues that lie on the imaginary axis, that is, those of L.

In the case $m = 1$, there are three important normal forms:

1. *Saddle-node bifurcation*: this corresponds to the case where the system (2.62), when reduced to its normal form, is

$$\frac{dx}{dt} = \lambda \pm x^2. \tag{2.63}$$

   The sign characterizes super-criticality ($\lambda - x^2$) or sub-criticality ($\lambda + x^2$). In the super-critical case, it is straightforward to check that the branch of solutions $x = \sqrt{\lambda}$ is linearly stable and the branch $x = -\sqrt{\lambda}$ is unstable (see Fig. 2.4).
2. *Trans-critical bifurcation*: in this case the normal form is given by

$$\frac{dx}{dt} = \lambda x \pm x^2. \tag{2.64}$$

   In both sub-critical and super-critical cases, there is an exchange of stability from stable to unstable fixed points and vice versa as the parameter λ is varied through the bifurcation at $\lambda = 0$ (see Fig. 2.5).
3. *Pitchfork bifurcation*: the normal form is

$$\frac{dx}{dt} = \lambda x \pm x^3. \tag{2.65}$$

   In the super-critical situation ($dx/dt = \lambda x - x^3$), there is a transfer of stability from the symmetric solution $x = 0$ to the pair of conjugated solutions $x = \pm\sqrt{\lambda}$

https://doi.org/10.1017/9781108863148.003 Published online by Cambridge University Press

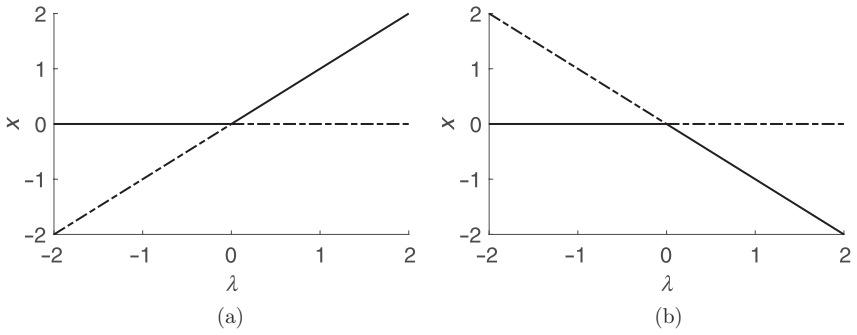

Figure 2.5 Super-critical (a) and sub-critical (b) trans-critical bifurcation.

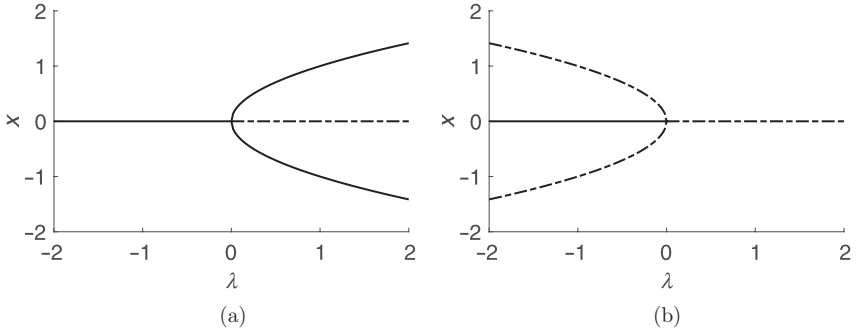

Figure 2.6 Super-critical (a) and sub-critical (b) pitchfork bifurcation.

(Fig. 2.6a). The system remains in a neighbourhood of the equilibrium so that one observes a soft or non-catastrophic loss of stability. In the sub-critical case ($dx/dt = \lambda x + x^3$), the situation is very different, as can be seen in Fig. 2.6b. The domain of attraction of the fixed point (the set of initial conditions which end up at the fixed point for infinite time) is bounded by the unstable fixed points and shrinks as the parameter λ approaches zero. The system is thus pushed out from the neighbourhood of the now unstable fixed point leading to a *sharp* or catastrophic loss of stability. Decreasing again the parameter to negative values will not necessarily return the system to the previously stable fixed point, since it may have already left its domain of attraction.

Whereas in cases 1–3, the number of fixed points changed as the parameter was varied, it is also possible that a steady solution becomes unstable to time-periodic disturbances. This so-called *Hopf bifurcation* occurs only in dynamical systems with $m > 1$ and corresponds to the special case of a simple conjugate pair of pure imaginary eigenvalues $\sigma = \pm i\omega$ crossing the imaginary axis, leading to the normal form (for $m = 2$)

https://doi.org/10.1017/9781108863148.003 Published online by Cambridge University Press

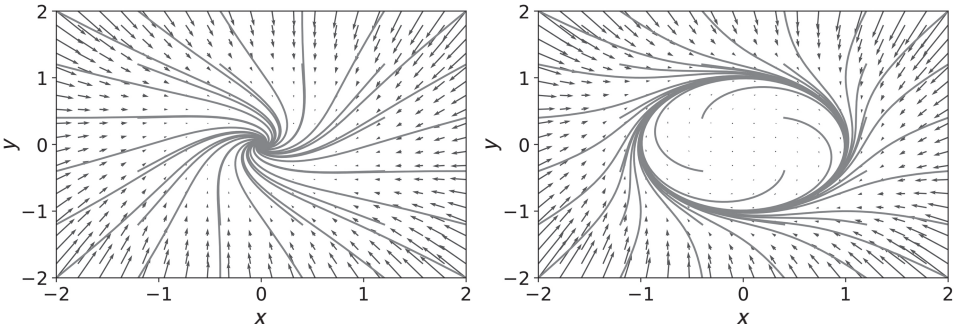

Figure 2.7 Phase portraits for a super-critical Hopf bifurcation (at $\lambda = 0$) where the arrows indicate the slope dy/dx at each location. (a) For $\lambda = -1 < 0$, there is only one stable fixed point. (b) A stable limit cycle $x^2 + y^2 = 1$ appears for $\lambda = 1 > 0$.

$$\frac{dx}{dt} = \lambda x - \omega y \pm x(x^2 + y^2), \tag{2.66a}$$

$$\frac{dy}{dt} = \omega x + \lambda y \pm y(x^2 + y^2). \tag{2.66b}$$

Phase portraits of the super-critical Hopf bifurcation ($-$ sign in (2.66)) show that for $\lambda < 0$, the fixed point ($x = 0, y = 0$) is stable (Fig. 2.7a). For $\lambda > 0$, a periodic orbit (with period $2\pi/\omega$) appears (Fig. 2.7b), which is called a *limit cycle* (an isolated periodic orbit).

The normal form (2.66) can also be written in polar coordinates $x = r\cos\theta, y = r\sin\theta$ as

$$\frac{dr}{dt} = \lambda r \pm r^3, \tag{2.67a}$$

$$\frac{d\theta}{dt} = \omega. \tag{2.67b}$$

Similar to the pitchfork bifurcation case, the sign determines whether the Hopf bifurcation is super-critical or sub-critical. *See example Ex. 2.4*

Example 2.1 *Consider the following particular case of the Ginzburg–Landau equation*

$$\frac{\partial A}{\partial t} = (\alpha + i\beta)A + \gamma_2 \frac{\partial^2 A}{\partial x^2} - \gamma_3 A|A|^2 \tag{2.68}$$

with real α, β, $\gamma_2 > 0$ and $\gamma_3 > 0$. Assume first that $\gamma_2 = 0$. To find an x-independent solution, which is called the Stokes wave, we substitute $A = \rho\exp(i\theta)$ into (2.68), where ρ and θ are both real. After cancelling the common factor $\exp(i\theta)$, one obtains the equation

https://doi.org/10.1017/9781108863148.003 Published online by Cambridge University Press

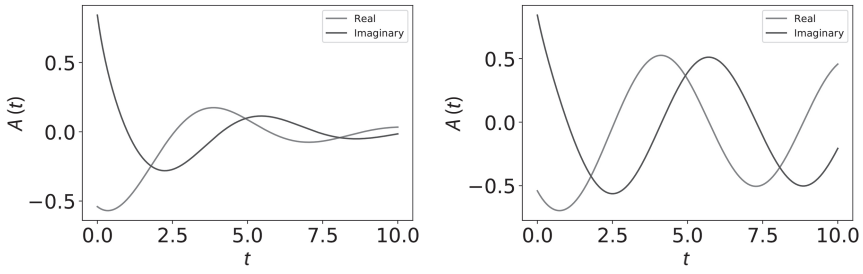

Figure 2.8 (a) Trajectories of (2.68) for $\gamma_2 = 0$, $\gamma_3 = 1$, $\beta = 1$ and values of (a) $\alpha = -0.25$ and (b) $\alpha = 0.25$.

$$\frac{d\rho}{dt} + i\rho\frac{d\theta}{dt} = i\rho\beta + \rho(\alpha - \gamma_3\rho^2). \tag{2.69}$$

Collecting real and imaginary parts, we obtain two equations:

$$\frac{d\rho}{dt} = \rho(\alpha - \gamma_3\rho^2), \tag{2.70a}$$

$$\frac{d\theta}{dt} = \beta. \tag{2.70b}$$

For $\alpha < 0$, the steady state $\bar{\rho} = 0$ is stable (Fig.2.8a). Clearly $\bar{\rho} = 0$ is unstable if $\alpha > 0$, but then stable states $\bar{\rho} = \sqrt{\alpha/\gamma_3}$ exist. For $\rho \neq 0$, θ is a linear function of t, that is, $\theta = c + \beta t$. So, the solution is

$$A = \sqrt{\alpha/\gamma_3}\exp(ic + i\beta t). \tag{2.71}$$

This periodic solution with period $2\pi/\beta$ is also a limit cycle for $\alpha > 0$ (Fig. 2.8b). Now, if we choose $\gamma_2 > 0$, then this has a stabilizing effect, so α needs to be larger than a certain positive value for the periodic solution to exist.

Additional Material

- The text in these sections is meant as a very short recap of dynamical systems theory. Other books are much more suitable to learn about this theory. Introductions with many examples can be found in Strogatz (1994), Verhulst (2000), and Perko (2013). More advanced texts are Guckenheimer and Holmes (1990) and Kuznetsov (1995).

2.5 Bifurcation Theory of Limit Cycles

In this section, we provide a brief overview of bifurcations of periodic orbits of autonomous dynamical systems when a single parameter is varied.

Assume that one has a limit cycle, say indicated by γ, of the original system (2.52) for a parameter λ that we omit in the notations for simplicity, and whose

https://doi.org/10.1017/9781108863148.003 Published online by Cambridge University Press

corresponding solution is $\bar{\mathbf{x}}(t) = \bar{\mathbf{x}}(t+p)$, where p is the period of the orbit. We consider an infinitesimal perturbation $\mathbf{y}(t)$ of γ, that is, we let $\mathbf{x}(t) = \bar{\mathbf{x}}(t) + \mathbf{y}(t)$ in (2.52), and neglecting quadratic terms, one then obtains

$$\dot{\mathbf{y}} = J(\bar{\mathbf{x}}(t))\mathbf{y}, \tag{2.72}$$

and $J(\bar{\mathbf{x}}(t))$ is a p-periodic matrix.

It can be shown (Guckenheimer and Holmes, 1990) that, using the fundamental solution matrix Y of the system (2.72), it follows that

$$Y(t+p) = \Phi Y(t). \tag{2.73}$$

With $Y(0) = I$, it follows that $\Phi = Y(T)$. The matrix Φ is called the monodromy matrix, and its eigenvalues $\rho_1, \ldots, \rho_d$ are called the Floquet multipliers. The monodromy matrix is not uniquely determined by the solutions of (2.72), but its eigenvalues are. Since the perturbation $\mathbf{y}(t) = \bar{\mathbf{x}}(t+\epsilon) - \bar{\mathbf{x}}(t)$, ϵ small, is p-periodic, it immediately implies that Φ has an eigenvalue $\rho_1 = +1$, that is, perturbations along γ neither diverge nor converge. The linear stability of γ is thus determined by the remaining $d-1$ eigenvalues.

Let Σ^+ be a (fixed) local cross section of dimension $d-1$ (see Fig. 2.3) of the limit cycle γ such that the periodic orbit is not tangent to this hypersurface, and denote $\mathbf{x}^\star$ the intersection of Σ^+ with γ. There is a nice geometrical interpretation of the monodromy matrix in terms of the Poincaré map defined as $\mathcal{P}(\mathbf{x}) = \phi_\tau(\mathbf{x})$, where $\mathbf{x}$ is assumed to be in a neighbourhood of $\mathbf{x}^\star$, and τ is the time taken for the orbit $\phi_t(\mathbf{x})$ to first return to Σ^+ (as $\mathbf{x}$ approaches $\mathbf{x}^\star$, τ will tend to p). After a change of basis such that the matrix Φ has a column $(0, \cdots 0, 1)^T$ corresponding to the unit eigenvalue, the remaining block $(d-1)\times(d-1)$ matrix corresponds to the linearized Poincaré map. These remarks show that the bifurcations of limit cycles are related to the behaviour of a discrete dynamical system (from the Poincaré map) $\mathbf{x}_{n+1} = \mathcal{P}\mathbf{x}_n$.

As an example, consider the system of equations for the supercritical Hopf bifurcation, in polar coordinates given by (2.67) as

$$\begin{aligned} \frac{dr}{dt} &= \lambda r - r^3, \\ \frac{d\theta}{dt} &= \omega. \end{aligned}$$

At $\lambda = 0$, a Hopf bifurcation occurs and, for $\lambda > 0$, a periodic orbit having a period $p = 2\pi/\omega$ exists and is described by

$$r = \sqrt{\lambda}\ ;\ \theta = \omega t. \tag{2.75}$$

https://doi.org/10.1017/9781108863148.003 Published online by Cambridge University Press

To determine the stability of the periodic orbit coming from (2.66) for $\lambda > 0$ and $\omega \neq 0$, we write the solution as

$$\bar{x}(t) = \sqrt{\lambda}\ \cos \omega t,$$
$$\bar{y}(t) = \sqrt{\lambda}\ \sin \omega t.$$

The Jacobian matrix at the periodic orbit can be obtained from (2.66) and is given by

$$J(\bar{\mathbf{x}}(t), \lambda) = \begin{pmatrix} \lambda - 3x^2(t) - y^2(t) & -\omega - 2x(t)y(t) \\ \omega - 2x(t)y(t) & \lambda - 3y^2(t) - x^2(t) \end{pmatrix}. \tag{2.76}$$

Next, to determine the monodromy matrix, the system $d\mathbf{y}_j/dt = J(\bar{\mathbf{x}}(t), \lambda)\mathbf{y}_j$ has to be solved for $j = 1, 2$ with $y_1(0) = (1, 0)$ and $y_2(0) = (0, 1)$ as initial conditions. This has to be done numerically, and the monodromy matrix Φ is found from

$$\Phi = (y_1(\frac{2\pi}{\omega}), y_2(\frac{2\pi}{\omega})). \tag{2.77}$$

The Floquet multipliers are determined as the two eigenvalues of the matrix Φ. The first one ($\rho_1 = 1$) is unity, and the second one determines the stability of the periodic orbit, and in this case it is within the unit circle ($\mid \rho_2 \mid < 1$) for $\lambda > 0$; so the periodic orbit is stable.

The value of ρ_2 can be analytically determined by first defining a Poincaré section (for certain θ_0) as

$$\Sigma^+ = \{(r, \theta) \in \mathbb{R} \times [0, 2\pi) \mid \theta = \theta_0\}. \tag{2.78}$$

In this case, the normal in polar coordinates is given by $\mathbf{n} = (0, 1)$ and (on the periodic orbit) $\mathbf{f} = (0, \omega)$ such that Σ^+ is a one-sided Poincaré section if $\omega \neq 0$. If we choose $\theta_0 = \pi/2$, then in Cartesian coordinates, the Poincaré section is parallel to the y-axis. For example, one could take the interval $y \in (0, 1]$ as a Poincaré section.

The Poincaré map can in this case be explicitly computed because explicit solutions exist of the trajectories for all initial conditions (r_0, θ_0) at $t = t_0$. Using the indefinite integral,

$$\int \frac{dx}{\alpha_1 x^3 + \alpha_2 x} = \frac{1}{2\alpha_2}\ \ln \mid \frac{x^2}{\alpha_1 x^2 + \alpha_2} \mid, \tag{2.79}$$

the closed-form solution $(r(t), \theta(t))$ is

$$\begin{aligned} r(t; t_0) &= \left[(\frac{1}{r_0^2} - \frac{1}{\lambda}) e^{-2\lambda(t-t_0)} + \frac{1}{\lambda} \right]^{-\frac{1}{2}}, \\ \theta(t; t_0) &= \omega(t - t_0) + \theta_0. \end{aligned}$$

https://doi.org/10.1017/9781108863148.003 Published online by Cambridge University Press

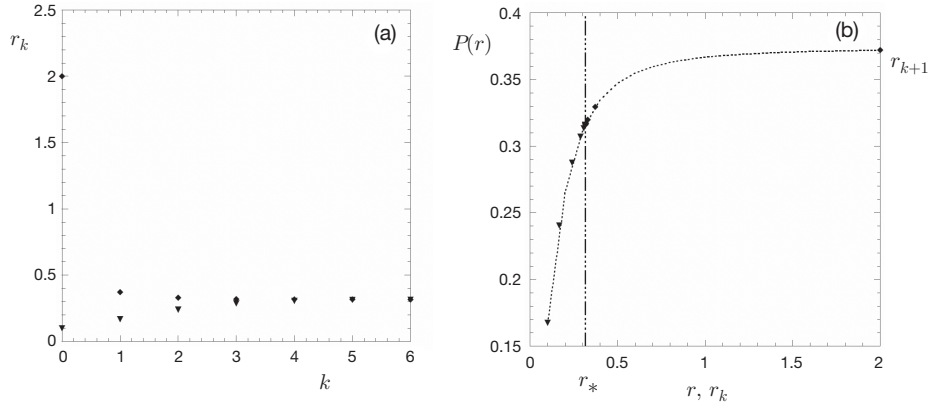

Figure 2.9 (a) Intersections r_k of the two trajectories for $\lambda = 0.1$ and $\omega = 1.0$ with the one-sided Poincaré section $r > 0, \theta_0 = \pi/2$. Subsequent intersections are labelled with k; the diamonds and triangles represent the intersections of the trajectories starting in (0,2) and (0,0.1), respectively. (b) Plot of the Poincaré map $\mathcal{P}(r)$ as in (2.81) together with the intersections r_k as in (a), but replotted as r_{k+1} versus r_k. The fixed point of the Poincaré map $\mathcal{P}(r)$ is at $r_* = \sqrt{\lambda} = 0.3162$.

A trajectory with initial conditions at (r_0, θ_0) intersects Σ^+ at times $t_k = t_0 + 2k\pi/\omega$. As the time difference between subsequent intersections (needed for the Poincaré map) is $2\pi/\omega$, this gives

$$r_{k+1} = \mathcal{P}(r_k) = \left[\left(\frac{1}{r_k^2} - \frac{1}{\lambda} \right) e^{\frac{-4\pi\lambda}{\omega}} + \frac{1}{\lambda} \right]^{-\frac{1}{2}}. \tag{2.81}$$

Fixed points of the Poincaré map $\mathcal{P}(r)$ are defined by $\mathcal{P}(r_*) = r_*$, and a short calculation gives that $r_* = \sqrt{\lambda}$. The Poincaré map $\mathcal{P}$ is plotted as the dotted curve in Fig. 2.9b for the case $\lambda = 0.1, \omega = 1$. The intersections r_k of the two trajectories with the Poincaré section defined by $r > 0, \theta_0 = \pi/2$ are plotted versus k (which monitors the subsequent intersections) in Fig. 2.9a. They are replotted in Fig. 2.9b as r_{k+1} versus r_k and indeed move along the Poincaré map; with increasing k, the fixed point r_* is reached. *See example Ex. 2.5*

To determine the stability of the periodic orbits, the stability of the fixed point of the Poincaré map is considered. The Jacobian of the Poincaré map will indicate whether intersections of trajectories drift away (if positive) or are attracted to (if negative) the fixed point of the Poincaré map. For the periodic orbit the stability can be determined from

$$\frac{d\mathcal{P}}{dr}(r = \sqrt{\lambda}) = \frac{d}{dr} \left[\left(\frac{1}{r^2} - \frac{1}{\lambda} \right) e^{\frac{-4\pi\lambda}{\omega}} + \frac{1}{\lambda} \right]^{-\frac{1}{2}} (r = \sqrt{\lambda}) = e^{\frac{-4\pi\lambda}{\omega}}. \tag{2.82}$$

https://doi.org/10.1017/9781108863148.003 Published online by Cambridge University Press

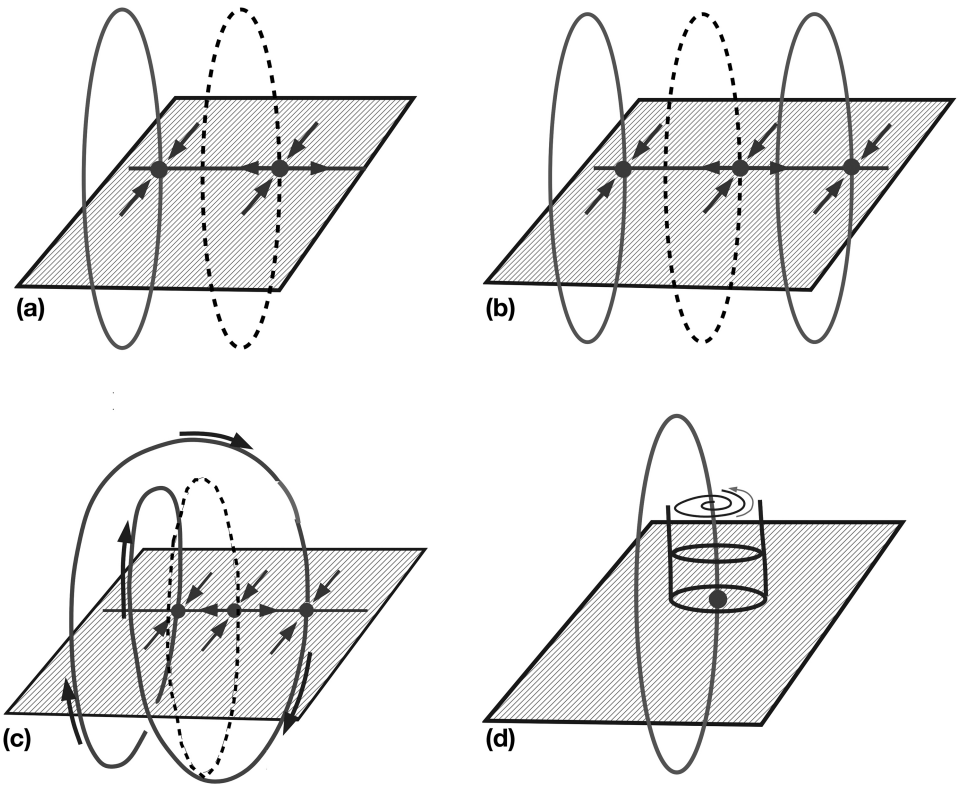

Figure 2.10 State space view associated with (a) a saddle-node and (b) a pitchfork bifurcation of a periodic orbit, (c) a period-doubling or flip bifurcation of a periodic orbit, and (d) a Neimark–Sacker or torus bifurcation. The original periodic orbit is shown as the dashed curve in (a), (b), and (c).

The norm of the right-hand side of this equation is smaller than unity for $\lambda > 0$ and hence the periodic orbit is stable.

The bifurcation theory for fixed points of the iterative map with an eigenvalue having unit norm is completely analogous to the bifurcation theory for fixed points of continuous systems with an eigenvalue on the imaginary axis. Periodic orbits become unstable when Floquet multipliers ρ_i cross the unit circle as the parameter λ is changed.

There are three important cases (Kuznetsov, 1995):

1. A real Floquet multiplier is crossing the unit circle $\rho(\bar{\lambda}) = 1$ at $\lambda = \bar{\lambda}$, which gives a saddle-node bifurcation of a periodic orbit, also called a cyclic-fold bifurcation (Fig. 2.10a). This situation can be shown to be topologically equivalent to the one-dimensional discrete dynamical system

$$x_{n+1} = \mathcal{P}(x_n), \text{ with } \mathcal{P}(x) = \lambda + x \pm x^2. \tag{2.83}$$

https://doi.org/10.1017/9781108863148.003 Published online by Cambridge University Press

Consider the super-critical case $\mathcal{P}(x) = \lambda + x - x^2$ and assume that $\bar{\lambda} = 0$ for simplicity. As λ becomes positive, two fixed points $x_1^\star$ and $x_2^\star$ of the iterative map (2.83) appear which are solutions of $\mathcal{P}(x) = x$. These two fixed points correspond to the appearance of two new families of periodic orbits. One family is stable ($\mathcal{P}'(x_1^\star) < 1$), while the other is unstable ($\mathcal{P}'(x_2^\star) > 1$). Like in the case of fixed points, particular constraints (such as symmetry) may lead to trans-critical or pitchfork bifurcations (see Fig. 2.10b).

2. A real Floquet multiplier is crossing the unit circle at $\lambda = \bar{\lambda}$ with $\rho(\bar{\lambda}) = -1$. This situation is called flip or period-doubling bifurcation and has no equivalent for fixed points. The system is topologically equivalent to

$$x_{n+1} = \mathcal{P}(x_n), \text{ with } \mathcal{P}(x) = -(1+\lambda)x \pm x^3. \tag{2.84}$$

This situation corresponds to the pitchfork case for the second iterate $\mathcal{P}^2$ map. Again consider (with $\bar{\lambda} = 0$) the super-critical case $\mathcal{P}(x) = -(1+\lambda)x + x^3$. As λ becomes positive, two fixed points of the second iterate $\mathcal{P}^2$ appear which are not fixed points of the first iterate. This means that another stable periodic orbit of period $2p$ arises, whereas the original periodic orbit γ becomes unstable (Fig. 2.10c). The corresponding trajectories alternate from one side of γ to the other along the direction of the eigenvector associated with the Floquet multiplier $\rho = -1$.

3. A pair of complex conjugate Floquet multipliers ρ crosses the unit circle at $\lambda = \bar{\lambda}$ such that $|\rho(\bar{\lambda})| = |e^{i\varphi}| = 1$. This bifurcation is called a Neimark–Sacker or torus bifurcation (Fig. 2.10d). If one assumes after reduction on a two-dimensional invariant manifold that $d\rho(\lambda)/d\lambda \neq 0$ at $\lambda = \bar{\lambda}$, then there is a change of coordinates such that the Poincaré map takes the following form in polar coordinates (r, θ):

$$\begin{aligned} \mathcal{P}_r(r,\theta) &= r + c(\lambda - \bar{\lambda})r + ar^3, \\ \mathcal{P}_\theta(r,\theta) &= \theta + \varphi + br^2, \end{aligned} \tag{2.85}$$

where a, b, and c are parameters. Provided $a \neq 0$, this normal form indicates that a closed curve generically bifurcates from the fixed point; this closed curve corresponds to a two-dimensional invariant torus.

2.6 Summary

- Based on the concept of asymptotic stability in the mean, fluid flows are either monotonically stable, globally stable, conditionally stable, or unstable.

https://doi.org/10.1017/9781108863148.003 Published online by Cambridge University Press

- The linear stability boundary provides sufficient conditions for instability and it can, in general, be computed by solving an eigenvalue problem. The energy stability boundary can be determined by solving a non-linear optimization problem (not discussed here).
- The non-linear behaviour of the flow near the linear stability boundary can be studied using weakly non-linear theory. If the geometry is unbounded in one direction, Ginzburg–Landau theory can be used. If not, the theory of amplitude equations can be used.
- Dynamical systems theory for finite-dimensional autonomous systems provides a framework to understand transition behaviour in fluid flows when parameters are changed. When only one parameter is involved, only four types of bifurcations occur: saddle-node, trans-critical, pitchfork, and Hopf bifurcations. The first three bifurcations lead to multi-stable systems, and the Hopf bifurcation leads to oscillatory behaviour.
- Periodic orbits in autonomous dynamical systems, such as those arising at Hopf bifurcations, can become unstable when a parameter is varied. Apart from saddle-node, trans-critical, and pitchfork bifurcations, period doubling and torus bifurcations also can occur.

2.7 Exercises

Exercise 2.1 *For the Rayleigh–Bénard convection problem, the so-called principle of exchange of stability holds, which states that the eigenvalue σ is real at criticality.*

a. Multiply (2.6a) with $\tilde{\mathbf{u}}$ and (2.6c) with $\tilde{\vartheta}$ and integrate the result over the flow domain, substitute solutions proportional to $e^{\sigma t}$, and derive an equation for the eigenvalue $\sigma = \sigma_R + i\sigma_I$.

b. Prove that $\sigma_I = 0$.

Exercise 2.2 *Consider the pure Bénard–Marangoni problem in a horizontally unbounded configuration, with $Ra = 0$, as discussed in Section 1.3.*

a. Show that the background solution for $Bi \to \infty$ is the same as that for the Rayleigh–Bénard problem.

b. Determine in this case, the critical value of Ma associated with the linear stability boundary as a function of k.

https://doi.org/10.1017/9781108863148.003 Published online by Cambridge University Press

Exercise 2.3 *A crucial step in the derivation of the Ginzburg–Landau equation (2.36) is the application of the Fredholm alternative to the singular non–self-adjoint system at $\mathcal{O}(\epsilon^3 E)$ and in particular the determination of the vector $\mathbf{\Omega}$ in (2.37). Numerically, this can be done by first computing a Singular Value Decomposition (SVD) of the linear operator as follows:*

$$i\omega_c \hat{M}(k_c) + \hat{L}(k_c) = WSV^H,$$

where $S = diag(s_1, \ldots, s_d)$ is the diagonal matrix of singular values with $s_d = 0$. The matrices W and V are orthonormal, and the superscript H indicates the Hermitian transpose.

Define $C = \sigma_d \hat{M} + \hat{L}$, where σ_d is the eigenvalue near criticality.

a. Show that $\mathbf{\Omega}$ can be determined efficiently from the problem

$$CC^H \mathbf{\Omega} = 0.$$

b. Show that in the Ginzburg–Landau equation, the coefficients $\gamma_i, i = 1, 2$ can be determined from

$$\gamma_1 = m\frac{\partial \sigma}{\partial \lambda}\ ;\ \gamma_2 = -\frac{1}{2}\frac{\partial^2 \sigma}{\partial k^2}.$$

c. How can the group velocity c_g be efficiently computed using the SVD given at the beginning of this exercise?

Exercise 2.4 *Consider the following system of equations:*

$$\begin{aligned} \frac{dA}{dt} &= AB - A, \\ \frac{dB}{dt} &= -A^2 - B + \gamma, \end{aligned}$$

for real functions $A(t)$ and $B(t)$ with $t \in [0, \infty)$; $\gamma \geq 0$ is a real number.

a. Determine the fixed points $(\bar{A}, \bar{B})$ of these equations with γ as a control parameter.

b. Determine the linear stability of the fixed points $(\bar{A}, \bar{B})$. What special phenomenon occurs at $\gamma = 9/8$ on the branches for which $\bar{A} \neq 0$?

Exercise 2.5 *With a scaling $\tau = \rho_* T$, $\chi = \eta X$, and $a(\chi, \tau) = a_\infty^{-1} A(X, T) exp(-im\omega_\lambda T)$, with*

$$\rho_* = m(\sigma_R)_\lambda\ ;\ \eta = \sqrt{-\frac{2m(\sigma_R)_\lambda}{(\sigma_R)_{kk}}}\ ;\ a_\infty = \sqrt{m\frac{(\sigma_R)_\lambda}{\mathcal{R}(\gamma_3)}},$$

https://doi.org/10.1017/9781108863148.003 Published online by Cambridge University Press

the Ginzburg–Landau (2.36) can be transformed into

$$\frac{\partial a}{\partial \tau} = a + (1 + i\alpha_1)\frac{\partial^2 a}{\partial \chi^2} - (1 + i\alpha_2)a|a|^2.$$

a. Show that the Ginzburg–Landau equation has only bounded solutions when $\mathcal{R}(\gamma_3) > 0$.

b. Determine the coefficients α_1 *and* α_2.

c. Determine the Stokes wave solution $a_S(\tau)$ *of the Ginzburg–Landau equation.*

https://doi.org/10.1017/9781108863148.003 Published online by Cambridge University Press